

HYPERSPECTRAL IMAGE RESTORATION VIA GLOBAL TOTAL VARIATION REGULARIZED LOCAL NONCONVEX LOW-RANK MATRIX APPROXIMATION

Haijin Zeng, Xiaozhen Xie*, Jifeng Ning

Northwest A&F University, College of Science, Yangling 712100, P.R. China

ABSTRACT

Several bandwise total variation (TV) regularized low-rank (LR)-based models have been proposed to remove mixed noise in hyperspectral images (HSIs). Conventionally, the rank of LR matrix is approximated using nuclear norm (NN). The NN is defined by adding all singular values together, which is essentially a L_1 -norm of the singular values. It results in non-negligible approximation errors and thus the resulting matrix estimator can be significantly biased. Moreover, these bandwise TV-based methods exploit the spatial information in a separate manner. To cope with these problems, we propose a spatialspectral TV (SSTV) regularized non-convex local LR matrix approximation (NonLLRTV) method to remove mixed noise in HSIs. From one aspect, local LR of HSIs is formulated using a non-convex L_γ -norm, which provides a closer approximation to the matrix rank than the traditional NN. From another aspect, HSIs are assumed to be piecewisely smooth in the global spatial domain. The TV regularization is effective in preserving the smoothness and removing Gaussian noise. These facts inspire the integration of the NonLLR with TV regularization. To address the limitations of bandwise TV, we use the SSTV regularization to simultaneously consider global spatial structure and spectral correlation of neighboring bands. Experiment results indicate that the use of local non-convex penalty and global SSTV can boost the preserving of spatial piecewise smoothness and overall structural information.

Index Terms— Hyperspectral images, restoration, non-convex, local low-rank, spatial-spectral total variation.

1. INTRODUCTION

Hyperspectral images (HSIs) can provide spectral information of hundreds of continuous bands in the same scene. They are widely used in many fields. In recent years, HSIs have attracted great research interest in the field of remote sensing. However, due to the limitations of observation conditions and sensors, the HSI obtained by hyperspectral imagers is usually

contaminated by a variety of noises, such as Gaussian noise, stripes, deadlines, and impulse noise. These noises adversely affect the image quality of HSIs, the subsequent processing and applications.

Low rank (LR) model is a powerful tool in image processing, and its purpose is to decompose the observation data into a low rank matrix representing ideal data and a sparse matrix representing sparse noise. Based on LR model, numerous approaches have been proposed for HSI restoration. Albeit the success of LR models in theoretical research and practical applications, they may obtain suboptimal performance in real applications, since the nuclear norm (NN) may not be a good approximation to the rank function. Specifically, compared to the rank function in which all the nonzero singular values have equal contributions, the NN treats the singular values differently by adding them together. Moreover, the theoretical requirements (e.g., incoherence property) of the NN are usually very hard to satisfy in practical scenarios. Recently, a number of studies, both practically and theoretically, have shown that non-convex penalty of LR can provide better estimation accuracy and variable selection consistency than NN [1]. Motivated by such facts, several non-convex penalties have been proposed and studied as alternatives to NN.

In this paper, we propose a global spatial-spectral total variation (SSTV) regularized local non-convex LR matrix approximation (NonLLRTV) method for HSI denoising. Specifically, the HSIs are first divided into overlapping patches. Then, from one aspect, the clean HSI patches have its underlying local LR property, even though the observed HSI data may not be globally LR due to outliers and non-Gaussian noise. According to this fact, in our model, the local LR of hyperspectral data is represented by the newly emerged nonconvex L_γ -norm [2], which provides a closer approximation to the matrix rank than the traditional NN. From another aspect, HSIs are assumed to be piecewisely smooth in the global spatial domain. The TV regularization is effective in preserving the spatial piecewise smoothness and removing Gaussian noise. These facts inspire the integration of the NonLLR with TV regularization. To address the limitations of bandwise TV, we use the SSTV regularization to simultaneously consider global spatial structure and spectral correlation of neighboring bands.

*Corresponding author: xiexzh@nwfau.edu.cn.

This work was supported by the Fundamental Research Funds for the Central Universities under Grant No. 2452019073 and the National Natural Science Foundation of China under Grant No. 61876153.

2. PROBLEM FORMULATION

On the context of HSIs, it is well known that each spectral characteristic can be represented by a linear combination of a small number of pure spectral endmembers. It means that the Casorati matrix (a matrix whose columns comprise vectorized bands of the HSI) \mathbf{L} of clean HSI \mathcal{L} can be decomposed into $\mathbf{L} = \mathbf{UV}$. Then, the image degradation model can be expressed as $\mathbf{O} = \mathbf{UV} + \mathbf{S} + \mathbf{N}$, where \mathbf{O} , \mathbf{S} , \mathbf{N} denote the observed HSI, sparse noise and Gaussian noise, respectively.

Unfortunately, matrix \mathbf{O} is a morbid matrix with a huge difference in the number of columns and rows, i.e., $mn \gg p$, which result in blurring and a loss of details. To alleviate this problem and effectively explore the local low rank structure of underlying HSI, we denoise HSI patch by patch and first define an operator $P_{i,j} : \mathcal{L} \rightarrow \mathbf{L}_{i,j}$. This binary operator $P_{i,j}$ is used to extract $m_1 \times n_1$ rows from HSI data $\mathcal{L} \in \mathbb{R}^{m \times n \times p}$, i.e., $\mathcal{L}_{i,j} = P_{i,j}(\mathcal{L}) = \mathbf{L}_{i,j}$, where the spatial size of $m_1 \times n_1$ is centralized at pixel (i, j) of HSI data, $m_1 n_1$ is approximately equal to p . $P_{i,j}^T$ is the inverse of $P_{i,j}$.

As [3], we assume that each element of $\mathcal{U}_{i,j} \in \mathbb{R}^{m_1 n_1 \times r}$, $\mathcal{V}_{i,j} \in \mathbb{R}^{r \times p}$ is sampled from the Gaussian distribution, the sparse error $\mathcal{S}_{i,j}$ is sampled from the Laplace distribution, and the noise $\mathcal{G}_{i,j}$ obeys a Gaussian distribution, i.e., $\mathcal{U}_{i,j} \sim \mathcal{N}(0, \lambda_u^{-1})$, $\mathcal{V}_{i,j} \sim \mathcal{N}(0, \lambda_v^{-1})$, $\mathcal{S}_{i,j} \sim \mathcal{L}(0, \lambda_s^{-1})$, $\mathcal{N}_{i,j} \sim \mathcal{N}(0, \lambda_g^{-1})$. By treating $\mathcal{U}_{i,j}$, $\mathcal{V}_{i,j}$, and $\mathcal{S}_{i,j}$ as model parameters, and $\lambda_u, \lambda_v, \lambda_s$, and λ_g as hyperparameters with fixed values, we use the Bayesian estimation to find $\mathcal{U}_{i,j}$, $\mathcal{V}_{i,j}$ and $\mathcal{S}_{i,j}$. Based on Bayes rule, we have the following MAP formulation:

$$\begin{aligned} & p(\mathcal{U}_{i,j}, \mathcal{V}_{i,j}, \mathcal{S}_{i,j} | \mathcal{O}_{i,j}, \lambda_u, \lambda_v, \lambda_s, \lambda_g) \propto \\ & p(\mathcal{O}_{i,j} | \mathcal{U}_{i,j}, \mathcal{V}_{i,j}, \mathcal{S}_{i,j}, \lambda_g) \\ & \cdot p(\mathcal{U}_{i,j} | \lambda_u) p(\mathcal{V}_{i,j} | \lambda_v) p(\mathcal{S}_{i,j} | \lambda_s). \end{aligned} \quad (1)$$

Substituting the distribution of each variable into formula (1), and then using the Lemma 6 in [4], we can get

$$\begin{aligned} & \arg \min_{\mathcal{L}_{i,j}, \mathcal{S}_{i,j} \in \mathbb{R}^{m_1 n_1 \times p}} \|\mathcal{L}_{i,j}\|_* + \lambda \|\mathcal{S}_{i,j}\|_1 \\ & \text{st } \|\mathcal{O}_{i,j} - \mathcal{L}_{i,j} - \mathcal{S}_{i,j}\|_F^2 \leq \varepsilon, \text{rank}(\mathcal{L}_{i,j}) \leq r. \end{aligned} \quad (2)$$

Because the non-convex L_γ -norm can provide a closer approximation to the matrix rank than the traditional nuclear norm $\|\cdot\|_*$, we use L_γ -norm to represent the LR of hyperspectral data in (2) and propose the non-convex local patch-based low-rank model (NonLLR):

$$\begin{aligned} & \arg \min_{\mathcal{L}_{i,j}, \mathcal{S}_{i,j}} \sum_{i,j} \|\mathcal{L}_{i,j}\|_\gamma + \lambda \|\mathcal{S}_{i,j}\|_1 \\ & \text{s.t. } \|\mathcal{O}_{i,j} - \mathcal{L}_{i,j} - \mathcal{S}_{i,j}\|_F^2 \leq \varepsilon, \text{rank}(\mathcal{L}_{i,j}) \leq r, \end{aligned} \quad (3)$$

where $\|\mathcal{L}_{i,j}\|_\gamma = \sum_{t=1}^{\min\{m_1 n_1, p\}} (1 - e^{-\sigma_t(\mathcal{L}_{i,j})/\gamma})$, $\sigma_t(\mathcal{L}_{i,j})$ is the t -th singular value of $\mathcal{L}_{i,j}$.

NonLLR (3) is a local model which exploits the local LR property of HSIs, while SSTV is a global model which studies

the correlations of spatial pixels and spectral bands. By combining the local low-rank and TV properties in both spatial and spectral domains, we propose the following NonLLRTV model

$$\begin{aligned} & \arg \min_{\mathcal{L}, \mathcal{S}} \sum_{i,j} \left(\|\mathcal{L}_{i,j}\|_\gamma + \lambda \|\mathcal{S}_{i,j}\|_1 \right) + \tau \|\mathcal{L}\|_{\text{SSTV}} \\ & \text{s.t. } \|\mathcal{O}_{i,j} - \mathcal{L}_{i,j} - \mathcal{S}_{i,j}\|_F^2 \leq \varepsilon, \text{rank}(\mathcal{L}_{i,j}) \leq r, \end{aligned} \quad (4)$$

where the SSTV is defined as

$$\begin{aligned} \|\mathcal{L}\|_{\text{SSTV}} := & \sum_{i,j,k} w_1 |l_{i,j,k} - l_{i,j,k-1}| + w_2 |l_{i,j,k} - l_{i,j-1,k}| \\ & + w_3 |l_{i,j,k} - l_{i-1,j,k}|, \end{aligned} \quad (5)$$

and w_1, w_2 and w_3 are weighting parameters.

3. PROPOSED ALGORITHMS

In this section, we use the alternating direction method of multipliers (ADMM) to solve the NonLLRTV model (4). Auxiliary variables $\mathcal{J}, \mathcal{X} \in \mathbb{R}^{m \times n \times p}$ are first introduced, and NonLLRTV model (4) can be rewritten as follows:

$$\begin{aligned} & \arg \min_{\mathcal{L}, \mathcal{S}, \mathcal{J}, \mathcal{X}} \sum_{i,j} \left(\|\mathcal{L}_{i,j}\|_\gamma + \lambda \|\mathcal{S}_{i,j}\|_1 \right) + \tau \|\mathcal{X}\|_{\text{SSTV}} \\ & \text{s.t. } \mathcal{J} = \mathcal{X}, \mathcal{L}_{i,j} = \mathcal{J}_{i,j}, \mathcal{U} = \mathbf{D}\mathcal{X} \\ & \|\mathcal{O}_{i,j} - \mathcal{L}_{i,j} - \mathcal{S}_{i,j}\|_F^2 \leq \varepsilon, \text{rank}(\mathcal{L}_{i,j}) \leq r, \end{aligned} \quad (6)$$

where $\mathbf{D} = [w_1 \mathbf{D}_1, w_2 \mathbf{D}_2, w_3 \mathbf{D}_3]$ is the forward finite-difference operator along the three modes. By using ALM and ADMM method, minimization (6) can be transformed into the following two subproblems in Section 3.1 and 3.3, where $\Lambda_{i,j}^{\mathcal{O}}, \Lambda_{i,j}^{\mathcal{L}}, \Lambda_{\mathcal{X}}$ and Λ are Lagrangian parameters and μ is the penalty parameter.

3.1. Local NonLLR optimization for $(\mathcal{L}, \mathcal{S})$

For the above optimization problem, we solve each patch separately and accumulate a weighted sum of $(\mathcal{L}_{i,j}, \mathcal{S}_{i,j})$ to reconstruct $(\mathcal{L}, \mathcal{S})$.

Let $\mathcal{T}_{i,j} = \frac{1}{2} (\mathcal{O}_{i,j} + \mathcal{J}_{i,j} - \mathcal{S}_{i,j} + (\Lambda_{i,j}^{\mathcal{O}} + \Lambda_{i,j}^{\mathcal{L}}) / \mu)$. Then, the optimum solution of $\mathcal{L}_{i,j}$ -subproblem can be efficiently obtained by the generalized weight singular value thresholding (WSVT) [5]:

$$\mathbf{L}_{i,j}^* = \mathbf{P} \mathbf{S}_{\frac{\nabla \phi}{\mu}}(\Sigma) \mathbf{Q}^T \quad (7)$$

where $\mathbf{T}_{i,j} = \mathbf{P} \Sigma \mathbf{Q}^T$ is the SVD of $\mathbf{T}_{i,j}$; $\mathbf{S}_{(\nabla \phi / \mu)}(\Sigma) = \text{diag} \{ \max(\Sigma_{nn} - (\nabla \phi(\sigma_n) / \mu), 0) \}$, and $\phi(x) = 1 - e^{x/\gamma}$.

With $\mathcal{L}_{i,j}$ fixed, the solution of $\mathcal{S}_{i,j}$ can be directly obtained by the soft-thresholding $\text{Soft}(\mathcal{M}_{i,j}, \lambda/\mu)$ operation:

$$\mathcal{S}_{i,j} = \text{sign}(\mathcal{M}_{i,j}) \max \{0, |\mathcal{M}_{i,j}| - \lambda/\mu\}, \quad (8)$$

where $\mathcal{M}_{i,j} = \mathcal{O}_{i,j} - \mathcal{L}_{i,j} + \Lambda_{i,j}^{\mathcal{O}} / \mu$.

3.2. Global SSTV regularized reconstruction problem for $(\mathcal{J}, \mathcal{X}, \mathcal{U})$

The subproblem for \mathcal{J} can be deduced as a convex function, which has the following closed-form solution:

$$\mathcal{J} = (\mathcal{X} - \Lambda_{\mathcal{X}}/\mu + \sum_{i,j} \mathbf{P}_{i,j}^T (\mathcal{L}_{i,j} + \Lambda_{i,j}^{\mathcal{L}}/\mu)) / \mathcal{R}, \quad (9)$$

where $\mathcal{R} = \mathbf{1} + \sum_{i,j} \mathbf{P}_{i,j}^T \mathbf{P}_{i,j}$.

With \mathcal{J} fixed, the subproblem of \mathcal{X} can be efficiently solved by the fast Fourier transform (FFT) method:

$$\mathcal{X} = \mathcal{F}^{-1} \left[\frac{\mathcal{F}((\mathcal{J} + \Lambda_{\mathcal{X}}/\mu) + \mathbf{D}^T(\mathcal{U} + \Lambda/\mu))}{1 + \sum_{i=1}^3 (\mathcal{F}(w_i \mathbf{D}_i))^2} \right], \quad (10)$$

where $\mathcal{F}(\cdot)$ denotes the FFT and \mathcal{F}^{-1} is the inverse transform; \mathbf{D}^T represents the adjoint operator of \mathbf{D} .

Let $\mathcal{Y} = [\mathcal{Y}_1, \mathcal{Y}_2, \mathcal{Y}_3]$ and $\mathcal{U} = [\mathcal{U}_1, \mathcal{U}_2, \mathcal{U}_3]$. Likewise, \mathcal{U} can be solved by the soft-thresholding operation in (8):

$$\mathcal{U}_t = \text{Soft}(w_t \mathbf{D}_t \mathcal{X} - \mathcal{Y}_t/\mu, \tau/\mu), t = 1, 2, 3. \quad (11)$$

3.3. Updating Lagrangian parameters $\Lambda_{i,j}^{\mathcal{O}}, \Lambda_{i,j}^{\mathcal{L}}$ and $\Lambda_{\mathcal{X}}$

$$\begin{cases} \Lambda_{i,j}^{\mathcal{O}} = \Lambda_{i,j}^{\mathcal{O}} + \mu(\mathcal{O}_{i,j} - \mathcal{L}_{i,j} - S_{i,j}), \\ \Lambda_{i,j}^{\mathcal{L}} = \Lambda_{i,j}^{\mathcal{L}} + \mu(\mathcal{L}_{i,j} - \mathcal{J}_{i,j}), \\ \Lambda_{\mathcal{X}} = \Lambda_{\mathcal{X}} + \mu(\mathcal{J} - \mathcal{X}), \\ \Lambda = \Lambda + \mu(\mathcal{U} - \mathbf{D}\mathcal{X}). \end{cases} \quad (12)$$

Algorithm 1 summarizes the optimization strategy of step-by-step iteration as above.

Algorithm 1 HSI restoration via NonLLRTV model.

Input: $m \times n \times p$ observed HSI \mathcal{O} , patch size $m_1 \times n_1$, stopping criterion ε , regularization parameters λ, τ, γ .

Output: Denoised image \mathcal{X} ;

- 1: Initialize: $\mathcal{L} = \mathcal{X} = \mathcal{S} = \mathcal{J} = 0$, $\Lambda_{i,j}^{\mathcal{O}} = \Lambda_{i,j}^{\mathcal{L}} = 0$, $\Lambda_{\mathcal{X}} = 0$, $\Lambda = 0$, $\mu = 10^{-2}$, $\mu_{\max} = 10^6$, $\rho = 1.5$, $\gamma \in (7 * 10^{-3}, 1.2 * 10^{-2})$; $w_1 = w_2 = 1$, $w_3 = 0.5$; $\lambda = 0.14$, $\tau = 0.03$ and $k = 0$.
 - 2: Update all patches $(\mathcal{L}_{i,j}, \mathcal{S}_{i,j})$ by (7) and (8) respectively;
 - 3: Update $\mathcal{J}, \mathcal{X}, \mathcal{U}$ by (9), (10), (11) respectively;
 - 4: Update the Lagrangian multipliers by (12);
 - 5: Update the penalty parameter by $\mu := \min(\rho\mu, \mu_{\max})$
 - 6: Check the convergence condition:
 - 7: $\max \left\{ \|\mathcal{O}_{i,j} - \mathcal{L}_{i,j}^{k+1} - \mathcal{S}_{i,j}^{k+1}\|_{\infty}, \|\mathcal{J}^{k+1} - \mathcal{X}^{k+1}\|_{\infty} \right\} \leq \varepsilon$.
-

4. EXPERIMENTS AND RESULTS

In order to verify the effectiveness of our proposed model for HSI restoration, four different methods are employed as

the benchmark in the experiments. Since the BM3D is only suitable to remove Gaussian noise, we implement them on HSIs which are preprocessed by the classical RPCA restoration method. The classical Indian Pines dataset is selected to apply simulated experiments. The parameters of the proposed model are given in Algorithm 1. To simulate noisy HSI data, we add several types of noise to the original HSI data.

Case 1: Gaussian noise and impulse noise are added to the HSI. The mean value of Gaussian noise is zero and the variance is 0.05, the percentage of impulse noise is 0.1;

Case 2: Noise type is the same as Case 1, the mean value of Gaussian noise is zero, while its variance and the percentage of impulse noise for each band is randomly selected from 0 to 0.2;

Case 3: Only Gaussian noise is added to the HSI, the mean value of Gaussian noise is zero and the variance for each band is randomly selected from 0 to 0.2;

Case 4: Based on Case 2, deadlines are additionally added from band 131 to band 160;

Case 5: Based on Case 2, stripes are additionally added from band 111 to band 140;

Case 6: Based on Case 2, the deadlines and stripes in Case 4 and Case 5 both are added to the HSI.

For visual evaluation, we show the 140-th band of the recovered HSI with the noise case 4 in Fig. 1. Compared to other models, it can be seen that the result of our NonLLRTV model is closest to the original reference image. In addition, in order to further compare the performance of the models, we show the spectral characteristics of the clean HSI and the restored HSI in Fig. 2. It is also clear that the spectral characteristics in results of our NonLLRTV model are also closest to ones in the true data.

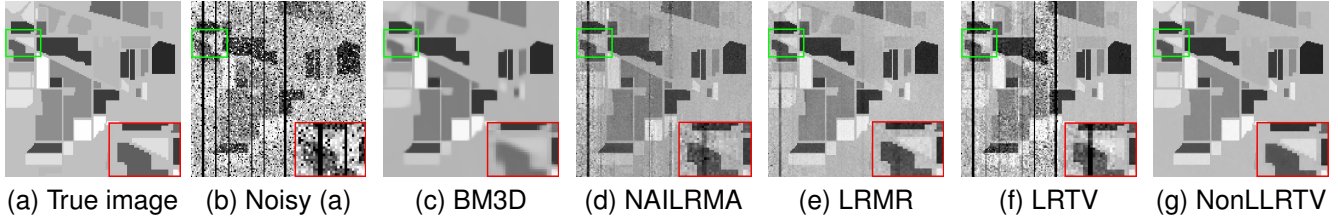
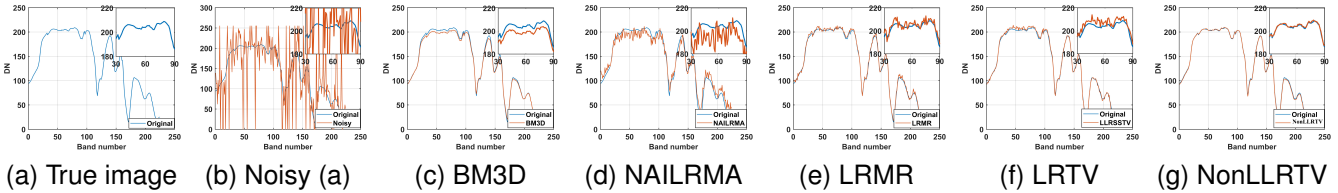
For quantitative comparison, Table 1 lists the PQIs of all the compared models in the six noise cases. The best results for each PQI are marked in bold. It is clear from Table 1 that in all cases our NonLLRTV model achieves the best results among all the test methods. It is worth noting that the NonLLRTV model is about 3.5 dB better in MPSNR compared to the suboptimal method.

5. CONCLUSION

In this paper, we investigated the restoration of HSI, and propose a spatialspectral TV regularized nonconvex local LR matrix approximation (NonLLRTV) method to remove mixed noise in HSIs. The mixed noise was simulated by using various combinations of Gaussian noise, impulse noise, stripes, and deadlines. Results on the Indian Pines dataset indicate that the use of local nonconvex penalty and global SSTV can boost the preserving of spatial piecewise smoothness and overall structural information. Our future steps include the investigation of other types and combinations of nonconvex penalties. Moreover, we will also investigate the use of these models on other high-dimensional data recovery.

Table 1. Quantitative evaluation of different methods in different noise cases of Indian Pines dataset

Noise	Evaluation index	BM3D [6]	NAILRMA [7]	LRMR [8]	LRTV [3]	NonLLRTV
Case 1	MPSNR/ MSSIM	28.676/ 0.945	24.295/ 0.768	33.757/ 0.892	34.497/ 0.886	37.564/ 0.982
Case 2	MPSNR/ MSSIM	28.779/ 0.946	28.190/ 0.841	33.986/ 0.893	35.642/ 0.904	38.805/ 0.986
Case 3	MPSNR/ MSSIM	29.277/ 0.949	37.144/ 0.937	35.320/ 0.911	35.854/ 0.903	40.219/ 0.989
Case 4	MPSNR/ MSSIM	28.718/ 0.946	28.089/ 0.841	33.679/ 0.891	35.258/ 0.899	38.435/ 0.985
Case 5	MPSNR/ MSSIM	28.647/ 0.946	27.467/ 0.826	33.523/ 0.890	34.854/ 0.910	38.394/ 0.986
Case 6	MPSNR/ MSSIM	28.573/ 0.945	27.412/ 0.831	33.207/ 0.886	34.271/ 0.900	38.131/ 0.985

**Fig. 1.** Restoration results in the 140-th band of Indian Pines dataset in Case 4. The PSNRs of (c)-(g) are 25.9026, 19.3116, 25.9038, 16.1044 and 35.1247, respectively.**Fig. 2.** Spectrum of pixel (110, 110) in the restoration results of Indian Pines dataset in Case 1.

6. REFERENCES

- [1] Zhaoran Wang, Han Liu, and Tong Zhang, "Optimal computational and statistical rates of convergence for sparse nonconvex learning problems," *Annals of statistics*, vol. 42, no. 6, pp. 2164, 2014.
- [2] Yongyong Chen, Yanwen Guo, Yongli Wang, Dong Wang, Chong Peng, and Guoping He, "Denoising of hyperspectral images using nonconvex low rank matrix approximation," *IEEE Transactions on Geoscience and Remote Sensing*, vol. 55, no. 9, pp. 5366–5380, 2017.
- [3] Wei He, Hongyan Zhang, Liangpei Zhang, and Huanfeng Shen, "Total-variation-regularized low-rank matrix factorization for hyperspectral image restoration," *IEEE transactions on geoscience and remote sensing*, vol. 54, no. 1, pp. 178–188, 2015.
- [4] Rahul Mazumder, Trevor Hastie, and Robert Tibshirani, "Spectral regularization algorithms for learning large incomplete matrices," *Journal of machine learning research*, vol. 11, no. Aug, pp. 2287–2322, 2010.
- [5] Stéphane Gaïffas and Guillaume Lécué, "Weighted algorithms for compressed sensing and matrix completion," *arXiv preprint arXiv:1107.1638*, 2011.
- [6] Kostadin Dabov, Alessandro Foi, Vladimir Katkovnik, and Karen Egiazarian, "Image denoising by sparse 3-d transform-domain collaborative filtering," *IEEE Transactions on image processing*, vol. 16, no. 8, pp. 2080–2095, 2007.
- [7] Wei He, Hongyan Zhang, Liangpei Zhang, and Huanfeng Shen, "Hyperspectral image denoising via noise-adjusted iterative low-rank matrix approximation," *IEEE Journal of Selected Topics in Applied Earth Observations and Remote Sensing*, vol. 8, no. 6, pp. 3050–3061, 2015.
- [8] Hongyan Zhang, Wei He, Liangpei Zhang, Huanfeng Shen, and Qiangqiang Yuan, "Hyperspectral image restoration using low-rank matrix recovery," *IEEE Transactions on Geoscience and Remote Sensing*, vol. 52, no. 8, pp. 4729–4743, 2013.